HHS Public Access

Author manuscript

Biotech Histochem. Author manuscript; available in PMC 2019 September 27.

Published in final edited form as:

Biotech Histochem. 2018 ; 93(8): 608–614. doi:10.1080/10520295.2018.1514466.

Osteopontin-targeted probe detects orthotopic breast cancers using optoacoustic imaging

A Samykutty[#],
Wake Forest School of Medicine, Department of Cancer Biology, 1 Medical Center Blvd, Winston-Salem, North Carolina 27157

A Thomas[#],
Wake Forest School of Medicine, Department of Internal Medicine, 1 Medical Center Blvd, Winston-Salem, North Carolina 27157

M McNally,
Wake Forest School of Medicine, Department of Cancer Biology, 1 Medical Center Blvd, Winston-Salem, North Carolina 27157

A Chiba, and
Wake Forest School of Medicine, Department of Surgery, 1 Medical Center Blvd, Winston-Salem, North Carolina 27157

LR McNally
Wake Forest School of Medicine, Department of Cancer Biology, 1 Medical Center Blvd, Winston-Salem, North Carolina 27157

[#] These authors contributed equally to this work.

Abstract

Improved detection of breast cancer using highly sensitive, tumor-specific imaging would facilitate diagnosis, surveillance and assessment of response to treatment. We conjugated osteopontin peptide to an infrared fluorescent dye to serve as a contrast agent for detection of breast cancer by multispectral optoacoustic tomography (MSOT). Selective binding of the osteopontin-based probe was identified using flow cytometry and near infrared fluorescent imaging in triple negative and HER2 positive breast cancer cell lines in vitro. Osteopontin-750 accumulation was evaluated in vivo using MSOT with secondary confirmation of signal accumulation using near infrared fluorescent imaging. The osteopontin-based probe demonstrated binding to breast cancer cells in vitro. Similarly, after intravenous administration of the osteopontin-750 probe, it accumulated preferentially in the subcutaneous breast tumor in nude mice (557 MSOT a.u. compared to untargeted organs such as kidney (53.7 MSOT a.u.) and liver (32.1 MSOT a.u.). At 2.5 h post-injection, signal intensity within the tumor was 9.7 and 17 times greater in the tumor bed than in the kidney or liver, respectively. Fluorescence imaging ex vivo comparing tumor signal to that of

Corresponding author: Lacey R. McNally, PhD, Associate Professor, Departments of Cancer Biology and Bioengineering, Wake Forest School of Medicine, Winston-Salem, NC 27157, 1-336-713-5161, lacey_mcnally@hotmail.com.
A Samykutty and A Thomas contributed equally to this work.

Declaration of interest
The authors report no conflicts of interest. The authors alone are responsible for the content and writing of this paper.

nontarget organs confirmed the results in vivo. MSOT imaging demonstrated selective accumulation of the fluorescent osteopontin targeting probe to tumor sites both in vitro and in vivo, and provided high-resolution images. Further development of this tool is promising for advanced diagnostic imaging, disease surveillance and therapeutic models that limit nontarget toxicity.

Keywords

breast cancer; contrast agent; multispectral optoacoustic tomography; osteopontin; targeted therapy

Breast cancer is a prevalent malignancy. In the United States in 2017, approximately 252,710 new cases of breast cancer were diagnosed and 40,610 deaths were reported (DeSantis et al. 2017). Although significant progress has been made in the care of patients with breast cancer (Park et al. 2015), the overall burden of disease from early stage disease to living with metastatic disease for increasing periods remains a significant public health issue (Coughlin and Ekwueme 2009). Advances in imaging that could enable improved diagnosis, disease measurement and assessment of treatment response have increasingly become a focus of research.

One approach to improving tumor-specific imaging in vivo is to employ a disease-specific protein with high binding affinity linked to a fluorescent radiolabel to create a targeted fluorescent probe that identifies tumors specifically (Ntziachristos et al. 2003). Detection of a fluorescent probe together with imaging enables direct visualization of the tumors (Bai and Bornhop 2012).

Precise localization of a fluorescent probe in vivo is a technical hurdle that hinders complete anatomic characterization of a tumor. Limitations of traditional two-dimensional planar imaging techniques include light scatter and signal attenuation, which decrease the ability of the fluorescent signal to distinguish internal anatomy (Leblond et al. 2010). Multispectral optoacoustic tomography (MSOT) provides high resolution images of tumors in vivo (McNally et al. 2016; Dey et al. 2018). MSOT overcomes the limitations of traditional imaging by exploiting a photoacoustic effect that enables highly specific separation of the fluorescent signal from the background signal, which produces cross-sectional images with resolutions of 75−150 μm (Razansky et al. 2012; Bhutiani et al. 2017).

Osteopontin, a multifunctional extracellular phosphoglycophosphoprotein, is expressed in bone and has been of interest increasingly as a potential diagnostic marker for cancer as well as a possible therapeutic target (Wei et al. 2017; Bandopadhyay et al. 2014). Recent work has begun to elucidate the role of osteopontin in early tumor biology including tumor development and growth, angiogenesis and metastasis (Coppola et al. 2004; Agrawal et al. 2002). Osteopontin is strongly expressed in breast cancer and has been shown to alter the tumor microenvironment (Sharon et al. 2015).

We investigated detection of breast cancer cells in vitro and in vivo using an osteopontin-labeled near infrared fluorescent probe that was detected using MSOT.

Material and methods

Cell culture

We used human breast cancer cell lines, triple negative (MDA-MB-231 and MDA-MB-468) and HER2 positive (SKBR3 and ZR-75–1), and an ovarian cancer cell line, CaOV3 (Kim et al. 2002), which is negative for osteopontin. Cells were grown at 37° C and 5% CO_2 in Dulbecco's modified Eagle medium (Life Technologies, Grand Island, NY) supplemented with 10% fetal bovine serum (Atlanta Biologicals, Lawrenceville, GA) and 1% L-glutamine (Life Technologies).

Labeling osteopontin with NIR dye

We combined 0.1 ml 25 mM phosphate buffer, pH 7.4, 3 μg osteopontin ligand (Prospec, Rehovat, Israel) and 50 nM water soluble Hilyte 750 succinyl ester dye (Anaspec, Fremont, CA) to form the dye-conjugated ligand probe. The probe then was transferred into dialysis tubing (2000 nominal molecular weight cut-off, NMWCO; Sigma-Aldrich, St. Louis, MO) and dialyzed against 25 mM phosphate buffer. Optical density was determined after conjugation of the Hilyte 750 succinyl ester dye with the osteopontin probe using a Jasco V-730 spectrophotometer (Jasco, Easton, MD).

Analysis of osteopontin probe binding in vitro

Human breast cell lines, MDA-MB-231, MDA-MB-468, SKBR3 and ZR-75–1 cells were plated in duplicate 6-well plates at 5.0×10^5/well at 37º C in 5% CO_2. Osteopontin-750 probe, 10 nM in 100 μl, was added for 2 h to each well. Osteopontin-750 probe was removed and cells were washed twice with phosphate-buffered saline (PBS) containing 10% fetal bovine serum prior to near infrared fluorescent imaging using AMI-HT (Spectral Imaging Instruments, Tucson, AZ) at an excitation of 710 nm and emission of 770 nm. Region of interest (ROI) measurements were acquired using AMI-View and values were compared by ANOVA using SAS 9.3 software (SAS Institute, Cary, NC).

Flow cytometry

We incubated 1 μM CF594 succinimidyl ester dye with 4 μg osteopontin in the dark for 2 h. The excess dye was dialyzed using dialysis bags. Then 10^6 breast cancer cells were blocked with 0.1% bovine serum albumin. The dye-bound osteopontin ligand was added to the breast cancer cells. The cells were incubated for 1 h in the dark, then the cells were centrifuged at 0.2 x g for 5 min. The supernatant was discarded and the pellets were re-suspended in 1 ml flow buffer (PBS 7.4 in 0.1% fetal bovine serum). The osteopontin level in breast cancer cells was determined using a BD Accuri C6 flow cytometer (Franklin lakes, NJ). Subsequent data analysis was performed using C Flow analysis (version 1.0.264.15) software (San Jose, CA).

Human breast cancer xenograft mouse models

We injected 2.0×10^6 MDA-MB-231 breast cancer cells into the mammary fat pad (orthotopically) of 4-week-old female athymic mice (Charles River, Raleigh, NC). Cells were suspended in 75 μl Dulbecco's modified essential medium (DMEM) cell culture

medium without fetal bovine serum. Tumor growth for 21 days produced tumors 4−5 mm in diameter before evaluation of the osteopontin-750 imaging probe. Mice were maintained on an alfalfa free diet (2920X; Envigo, Indianapolis, IN) with access to water *ad libitum.*

Near Infrared fluorescent imaging

Osteopontin-750 probe was administered intravenously at a concentration of 50 nM. Mice were anesthetized using 2.0% isoflurane and 1.0 l oxygen followed by near infrared fluorescence imaging with the AMI-HT to confirm systemic injection of osteopontin-750, then imaged after 2 h. Of the five mice initially injected and screened for near infrared fluorescence signal from breast tumors, three mice were selected for MSOT imaging based upon near infrared fluorescent signal intensity.

Evaluation of probe binding with MSOT

Mice were imaged using an inVision 512 MSOT (iThera Medical, Munich, Germany) 2.5 h after administration of the osteopontin-750 probe. Mice were imaged ventral side up in an animal holder and positioned in a nose cone for delivery of anesthesia. Anesthesia was maintained at 1.5% isoflurane in 0.8 l medical air and 0.1 l O_2 throughout imaging. Imaging was performed in the MSOT system using axial slices with a 0.3 mm step for 1.0 cm of the abdominal region containing the tumor, at wavelengths of 680, 700, 730, 750, 760, 770, 800, 850, 900 nm for each position using 20 averages/wavelength with acquisition time of 10 μsec/frame to minimize the influence of animal movement in the images (Kimbrough et al. 2015; Zeiderman et al. 2016). Slices were screened using a live preview multispectral signal (MSP). Respiration rate and signs of distress were monitored through all stages of the imaging procedure. After MSOT imaging, animals were euthanized by CO_2 overdose and cervical dislocation. Breast tumor, kidney, liver and spleen were removed and imaged using the AMI-HT as described below to confirm accumulation of the probe.

Image reconstruction and analysis

Reconstruction was performed using back-projection at a resolution of 75 μm and multispectral processing was performed using linear regression in the ViewMSOT software version 3.8 (iThera Medical) (Bhutiani et al. 2017). A ROI method was used to determine signal strength in the tumor, liver and kidney using ViewMSOT software and reported as MSOT a.u. The ROI for the osteopontin-750 probe intensity analysis was plotted over each organ according to the signal location as observed on MSOT and was kept constant for all image slices. The ROI analysis of osteopontin-750 probe was compared among organs using the ANOVA statistical test using SAS 9.3 software (SAS Institute, Cary, NC).

Organ analysis ex vivo using near infrared imaging

After MSOT imaging for 2.5 h (3 h post-injection of osteopontin-750), mice were euthanized and signal accumulation within the tumor was compared to nontarget organs, i.e., liver, kidney and spleen, using near infrared fluorescent imaging using AMI-HT. ROI analysis for each organ and each mouse was conducted using AMI-View software. Values were compared using ANOVA among mice and organs using SAS.

Results

Osteopontin probe binding was assessed by near infrared fluorescent imaging and flow cytometry. The osteopontin-750 probe exhibited uptake in both the triple negative and HER2 positive breast cancer cells; uptake was significantly greater in the triple negative cells compared to the HER2 positive cells (Figure 1). The osteopontin probe exhibited significant binding in both MDA-MB-468 (25.7 ± 2.5, $p = 0.016$) and MDA-MB-231 cells (27.6 ± 5.4, $p = 0.0337$) compared to control CaOv3 cells (0.4 ± 3.0) measured by flow cytometry in vitro (Figure 2).

Both near infrared fluorescence and MSOT imaging in vivo exhibited significant accumulation of osteopontin-750 within the tumor (Figures 3–6). Furthermore, the tomographic capability of the MSOT device enabled detection of biodistribution of the osteopontin-750 probe in a three dimensional orientation; accumulation appeared to be significantly greater in the tumor than in nontarget organs (Figure 3).

To localize probe signal precisely and to assess its relation to adjacent structures, cross-sectional images were obtained from 0.3 mm slices that included the tumor bed, liver and kidneys (Figures 4–5). ROI analysis was performed for all stacked slices to generate comparisons of signal intensity in each organ over the length of the mouse. Osteopontin-750 accumulation for each of the three mice is shown in Figure 5. Peak accumulation occurred at 2.5 h and mean signal intensity in the tumor was 9.7 times greater within the tumor (average for three tumors = 557.1 a.u. than in kidney (57.3 a.u.) $p = 0.0001$ and 17 times greater within the tumor than in liver 32.1 a.u. ($p = 0.0001$).

After imaging, several mice were sacrificed at 3 h post-injection and near infrared fluorescent imaging was performed ex vivo to verify osteopontin-750 probe accumulation within organs. As anticipated, the osteopontin-750 probe accumulated specifically within the breast tumors in each of the three mice (Figures 3–6) compared to liver ($p < 0.05$) and the untargeted osteopontin-750 probe was cleared by the kidneys as demonstrated by a signal within the kidney that also appeared in the liver (Figures 4–6).

The ROI analysis of the osteopontin-750 probe signal intensity revealed a signal of 4.6×10^9 photons/sec in the tumor compared to kidney (4.7×10^8 photons/sec), liver (2.5×10^8 photons/sec) and spleen (2.0×10^8 photons/sec) (Figure 6).

Discussion

We labeled and identified breast cancers in vivo using a murine model and an osteopontin-based probe that was detectable using both optoacoustic and near infrared fluorescent imaging. Our findings in vitro confirmed our findings in vivo that our probe accumulated selectively in the breast tumor. Although osteopontin-750 accumulated significantly within the breast tumor, the osteopontin-750 probe was cleared by the kidneys as evidenced by signal within the bladder and kidneys.

Our findings add to the body of evidence that MSOT can be used to detect breast cancer in both murine models (Quiros-Gonzalez et al. 2018) and humans (Becker et al. 2018; Diot et

al. 2017). To our knowledge, ours is the first report of successful breast tumor identification using a ligand-based contrast agent in conjunction with MSOT imaging. Others have used osteopontin as a target for disease detection including models for evaluating an osteopontin-directed antibody to study cardiac atherosclerosis (Qiao et al. 2017) and an electrochemical RNA-aptasensor to evaluate osteopontin in the plasma of patients with recurrent or metastatic breast cancer (Meirinho et al. 2017).

We used MDA-MB-231 cell lines that exhibited an intermediate range of expression of osteopontin in vitro. Other investigators have reported that triple negative breast cancers, such as MDA-MB-231, exhibit elevated levels of osteopontin; all human breast tumors that we used demonstrated some level of expression of this protein (Wang et al. 2008). A possible potential advantage of using an osteopontin label is that it does not rely on human epidermal growth factor-2 receptor (HER2) or hormone receptors, both of which have important predictive value for breast cancer, but are expressed only in subsets of patients. A protein with nearly ubiquitous distribution would enable assessment of the full spectrum of breast cancers, including triple negative breast cancer as well as metastatic disease, where different sites can develop over time and often demonstrate heterogeneous hormone and HER2 receptor status (Paoletti et al. 2018; Fribbens et al. 2018).

Our findings demonstrated the potential to bind a near infrared fluorescent molecule to an osteopontin targeting probe for breast tumor detection by both MSOT and near infrared fluorescence imaging. This technique also has promise for tumor-specific delivery of therapeutic agents. Such a system could limit nontarget treatment toxicity in the manner of antibody-drug conjugates including trastuzumab emtansine and sacituzumab govitecan among others (Alley et al. 2010; Ocean et al. 2017).

It is important that the presence of osteopontin in breast cancer appears to be a negative prognostic marker (Zduniak et al. 2015; Xu et al. 2015); some investigators propose that inhibition of osteopontin is a promising therapeutic option for cancer treatment (Wei et al. 2017). Clearly, further study of osteopontin-labeled probes as possible therapeutic systems is warranted. One might also envision a co-labeled system that carries both diagnostic and therapeutic agents that enable concurrent treatment and response assessment.

Important limitations of our study include the fact that we evaluated limited numbers of triple negative and HER2 positive breast cancer cell lines. Future work should be directed toward confirming our results throughout the spectrum of breast cancers.

We report here the successful selective identification of breast tumors in vitro and in vivo using a fluorescent probe that targets osteopontin that is detected by MSOT. Systems such as these are potentially significant for diagnostic, surveillance and therapeutic advances in the care of patients with breast cancer.

Acknowledgments

Funding

This work was supported by NIH grants R01CA202350, R01CA205941, R01EB020125, and the Nealie Belk Stevens Fund for Breast Cancer Research.

References

AGRAWAL D, CHEN T, IRBY R, QUACKENBUSH J, CHAMBERS AF, SZABO M, CANTOR A, COPPOLA D & YEATMAN TJ 2002 Osteopontin identified as lead marker of colon cancer progression, using pooled sample expression profiling. J Natl Cancer Inst, 94, 513–21. [PubMed: 11929952]

ALLEY SC, OKELEY NM & SENTER PD 2010 Antibody-drug conjugates: targeted drug delivery for cancer. Curr Opin Chem Biol, 14, 529–37. [PubMed: 20643572]

BAI M & BORNHOP DJ 2012 Recent advances in receptor-targeted fluorescent probes for in vivo cancer imaging. Curr Med Chem, 19, 4742–58. [PubMed: 22873663]

BANDOPADHYAY M, BULBULE A, BUTTI R, CHAKRABORTY G, GHORPADE P, GHOSH P, GORAIN M, KALE S, KUMAR D, KUMAR S, TOTAKURA KV, ROY G, SHARMA P, SHETTI D, SOUNDARARAJAN G, THORAT D, TOMAR D, NALUKURTHI R, RAJA R, MISHRA R, YADAV AS & KUNDU GC 2014 Osteopontin as a therapeutic target for cancer. Expert Opin Ther Targets, 18, 883–95. [PubMed: 24899149]

BECKER A, MASTHOFF M, CLAUSSEN J, FORD SJ, ROLL W, BURG M, BARTH PJ, HEINDEL W, SCHAFERS M, EISENBLATTER M & WILDGRUBER M 2018 Multispectral optoacoustic tomography of the human breast: characterisation of healthy tissue and malignant lesions using a hybrid ultrasound-optoacoustic approach. Eur Radiol, 28, 602–609. [PubMed: 28786007]

BHUTIANI N, KIMBROUGH CW, BURTON NC, MORSCHER S, EGGER M, MCMASTERS K, WOLOSZYNSKA-READ A, EL-BAZ A & MCNALLY LR 2017 Detection of microspheres in vivo using multispectral optoacoustic tomography. Biotech Histochem, 92, 1–6.

COPPOLA D, SZABO M, BOULWARE D, MURACA P, ALSARRAJ M, CHAMBERS AF & YEATMAN TJ 2004 Correlation of osteopontin protein expression and pathological stage across a wide variety of tumor histologies. Clin Cancer Res, 10, 184–90. [PubMed: 14734468]

COUGHLIN SS & EKWUEME DU 2009 Breast cancer as a global health concern. Cancer Epidemiol, 33, 315–8. [PubMed: 19896917]

DESANTIS CE, MA J, GODING SAUER A, NEWMAN LA & JEMAL A 2017 Breast cancer statistics, 2017, racial disparity in mortality by state. CA Cancer J Clin

DEY S, KUMARI S, KALAINAYAKAN SP, CAMPBELL III J, GHOSH P, ZHOU H, FITZGERALD KE, LI M, MASON RP & ZHANG L 2018 The vascular disrupting agent combretastatin A-4 phosphate causes prolonged elevation of proteins involved in heme flux and function in resistant tumor cells. Oncotarget, 9, 4090. [PubMed: 29423106]

DIOT G, METZ S, NOSKE A, LIAPIS E, SCHROEDER B, OVSEPIAN SV, MEIER R, RUMMENY E & NTZIACHRISTOS V 2017 Multispectral Optoacoustic Tomography (MSOT) of Human Breast Cancer. Clin Cancer Res, 23, 6912–6922. [PubMed: 28899968]

FRIBBENS C, GARCIA MURILLAS I, BEANEY M, HREBIEN S, O'LEARY B, KILBURN L, HOWARTH K, EPSTEIN M, GREEN E, ROSENFELD N, RING A, JOHNSTON S & TURNER N 2018 Tracking evolution of aromatase inhibitor resistance with circulating tumour DNA analysis in metastatic breast cancer. Ann Oncol, 29, 145–153. [PubMed: 29045530]

KIM J-H, SKATES SJ, UEDE T, WONG K-K, SCHORGE JO, FELTMATE CM, BERKOWITZ RS, CRAMER DW & MOK SC 2002 Osteopontin as a potential diagnostic biomarker for ovarian cancer. Jama, 287, 1671–1679. [PubMed: 11926891]

KIMBROUGH CW, KHANAL A, ZEIDERMAN M, KHANAL BR, BURTON NC, MCMASTERS KM, VICKERS SM, GRIZZLE WE & MCNALLY LR 2015 Targeting acidity in pancreatic adenocarcinoma: multispectral optoacoustic tomography detects ph-low insertion peptide probes in vivo. Clinical Cancer Research, 21, 4576–4585. [PubMed: 26124201]

LEBLOND F, DAVIS SC, VALDES PA & POGUE BW 2010 Pre-clinical whole-body fluorescence imaging: Review of instruments, methods and applications. J Photochem Photobiol B, 98, 77–94. [PubMed: 20031443]

MCNALLY LR, MEZERA M, MORGAN DE, FREDERICK PJ, YANG ES, ELTOUM IE & GRIZZLE WE 2016 Current and Emerging Clinical Applications of Multispectral Optoacoustic Tomography (MSOT) in Oncology. Clin Cancer Res

MEIRINHO SG, DIAS LG, PERES AM & RODRIGUES LR 2017 Electrochemical aptasensor for human osteopontin detection using a DNA aptamer selected by SELEX. Anal Chim Acta, 987, 25–37. [PubMed: 28916037]

NTZIACHRISTOS V, BREMER C & WEISSLEDER R 2003 Fluorescence imaging with near-infrared light: new technological advances that enable in vivo molecular imaging. Eur Radiol, 13, 195–208. [PubMed: 12541130]

OCEAN AJ, STARODUB AN, BARDIA A, VAHDAT LT, ISAKOFF SJ, GUARINO M, MESSERSMITH WA, PICOZZI VJ, MAYER IA, WEGENER WA, MALIAKAL P, GOVINDAN SV, SHARKEY RM & GOLDENBERG DM 2017 Sacituzumab govitecan (IMMU-132), an anti-Trop-2-SN-38 antibody-drug conjugate for the treatment of diverse epithelial cancers: Safety and pharmacokinetics. Cancer, 123, 3843–3854. [PubMed: 28558150]

PAOLETTI C, CANI AK, LARIOS JM, HOVELSON DH, AUNG K, DARGA EP, CANNELL EM, BARATTA PJ, LIU CJ, CHU D, YAZDANI M, BLEVINS AR, SERO V, TOKUDOME N, THOMAS DG, GERSCH C, SCHOTT AF, WU YM, LONIGRO R, ROBINSON DR, CHINNAIYAN AM, BISCHOFF FZ, JOHNSON MD, PARK BH, HAYES DF, RAE JM & TOMLINS SA 2018 Comprehensive Mutation and Copy Number Profiling in Archived Circulating Breast Cancer Tumor Cells Documents Heterogeneous Resistance Mechanisms. Cancer Res, 78, 1110–1122. [PubMed: 29233927]

PARK JH, ANDERSON WF & GAIL MH 2015 Improvements in US Breast Cancer Survival and Proportion Explained by Tumor Size and Estrogen-Receptor Status. J Clin Oncol, 33, 2870–6. [PubMed: 26195709]

QIAO R, QIAO H, ZHANG Y, WANG Y, CHI C, TIAN J, ZHANG L, CAO F & GAO M 2017 Molecular Imaging of Vulnerable Atherosclerotic Plaques in Vivo with Osteopontin-Specific Upconversion Nanoprobes. ACS Nano, 11, 1816–1825. [PubMed: 28121134]

QUIROS-GONZALEZ I, TOMASZEWSKI MR, AITKEN SJ, ANSEL-BOLLEPALLI L, MCDUFFUS LA, GILL M, HACKER L, BRUNKER J & BOHNDIEK SE 2018 Optoacoustics delineates murine breast cancer models displaying angiogenesis and vascular mimicry. Br J Cancer, 118, 1098–1106. [PubMed: 29576623]

RAZANSKY D, DELIOLANIS NC, VINEGONI C & NTZIACHRISTOS V 2012 Deep tissue optical and optoacoustic molecular imaging technologies for pre-clinical research and drug discovery. Curr Pharm Biotechnol, 13, 504–22. [PubMed: 22216767]

SHARON Y, RAZ Y, COHEN N, BEN-SHMUEL A, SCHWARTZ H, GEIGER T & EREZ N 2015 Tumor-derived osteopontin reprograms normal mammary fibroblasts to promote inflammation and tumor growth in breast cancer. Cancer Res, 75, 963–73. [PubMed: 25600648]

WANG X, CHAO L, MA G, CHEN L, TIAN B, ZANG Y & SUN J 2008 Increased expression of osteopontin in patients with triple-negative breast cancer. Eur J Clin Invest, 38, 438–46. [PubMed: 18452545]

WEI R, WONG JPC & KWOK HF 2017 Osteopontin -- a promising biomarker for cancer therapy. J Cancer, 8, 2173–2183. [PubMed: 28819419]

XU YY, ZHANG YY, LU WF, MI YJ & CHEN YQ 2015 Prognostic value of osteopontin expression in breast cancer: A meta-analysis. Mol Clin Oncol, 3, 357–362. [PubMed: 25798267]

ZDUNIAK K, ZIOLKOWSKI P, AHLIN C, AGRAWAL A, AGRAWAL S, BLOMQVIST C, FJALLSKOG ML & WEBER GF 2015 Nuclear osteopontin-c is a prognostic breast cancer marker. Br J Cancer, 112, 729–38. [PubMed: 25625274]

ZEIDERMAN MR, MORGAN DE, CHRISTEIN JD, GRIZZLE WE, MCMASTERS KM & MCNALLY LR 2016 Acidic pH-Targeted Chitosan-Capped Mesoporous Silica Coated Gold Nanorods Facilitate Detection of Pancreatic Tumors via Multispectral Optoacoustic Tomography. Acs Biomaterials Science & Engineering, 2, 1108–1120. [PubMed: 28626793]

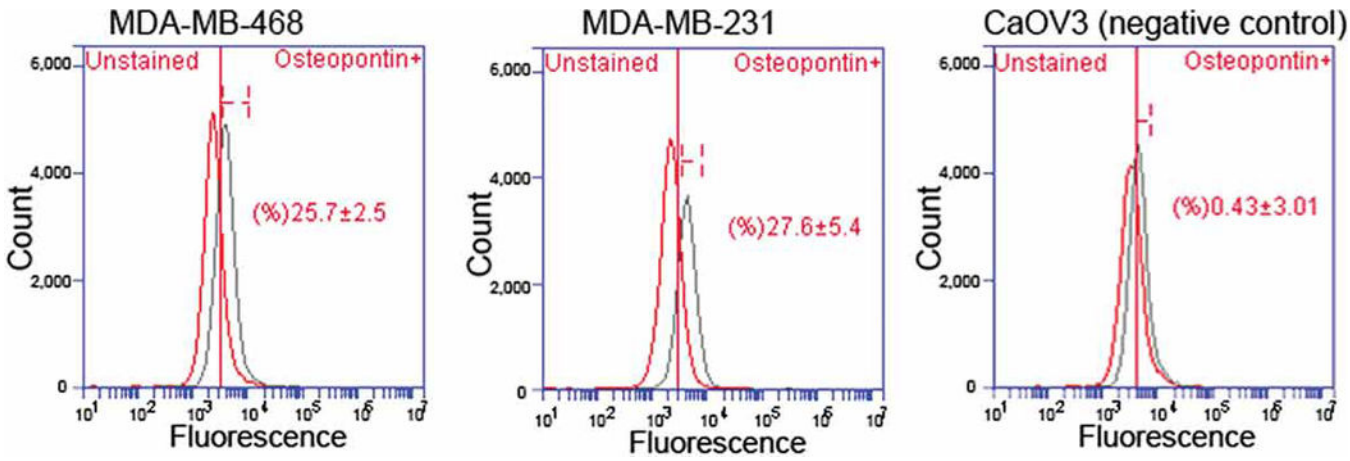

Figure 1.

Flow cytometry. MDA-MB-468 and MDA-MB-231 breast cancer cells and CaOV3 negative control cells stained with osteopontin-conjugated CF594 succinimidyl ester dye. Osteopontin expression in MDA-MB-231 (27.6 ± 5.4, $p = 0.0337$), MDA-MB-468 (25.7 ± 2.5, $p = 0.0161$) breast cancer cells were compared to the least expressing osteopontin CaOV3 cells.

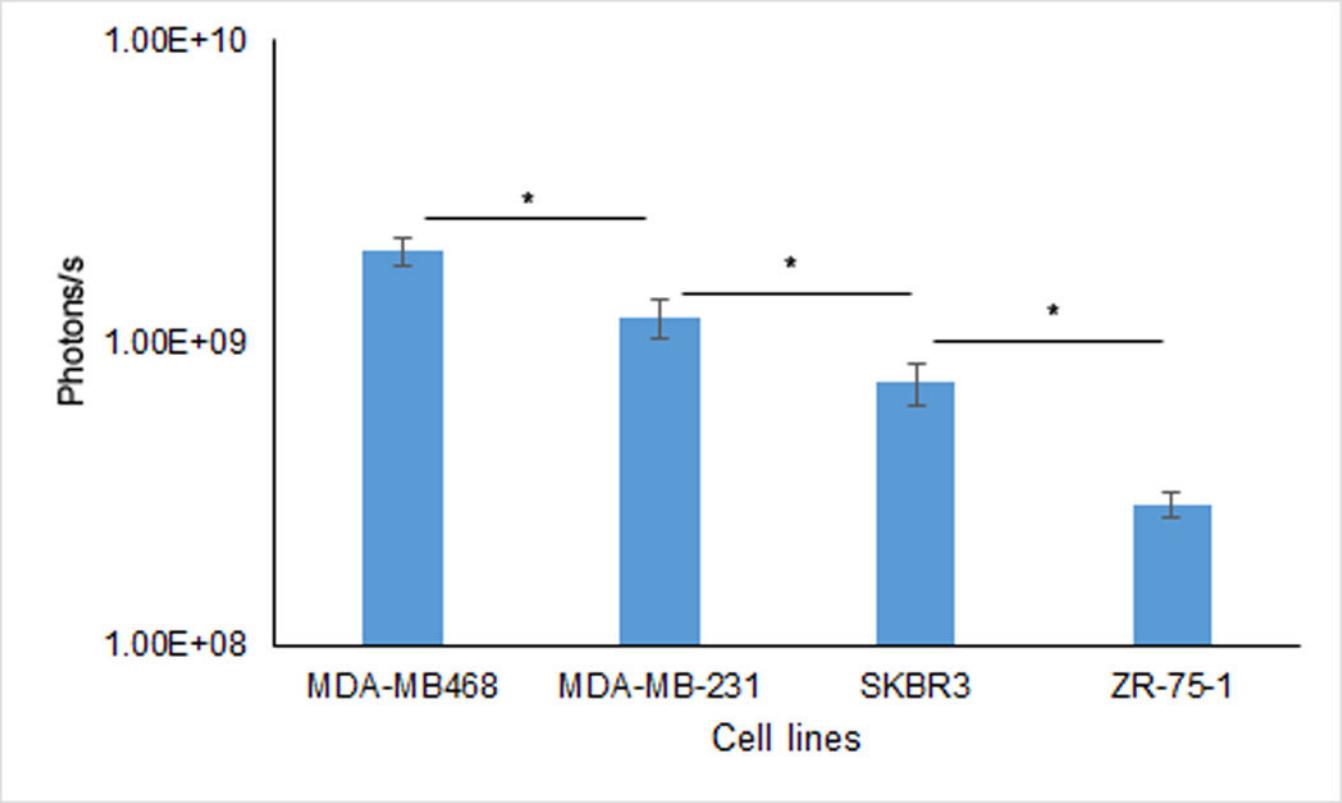

Figure 2.

Near infrared fluorescent imaging in vitro. Osteopontin-750 probe uptake into breast cancer cell lines was evaluated using AMI-HT. Images were acquired using 710 nm excitation and 770 nm emission filters. ROI data are means. Both triple negative breast cell lines, MDA-MB-468 and MDA-MB-231 exhibited greater uptake of osteopontin-750 than the HER2 positive breast cell lines, SKBR3 and ZR-75–1 ($p < 0.05$).

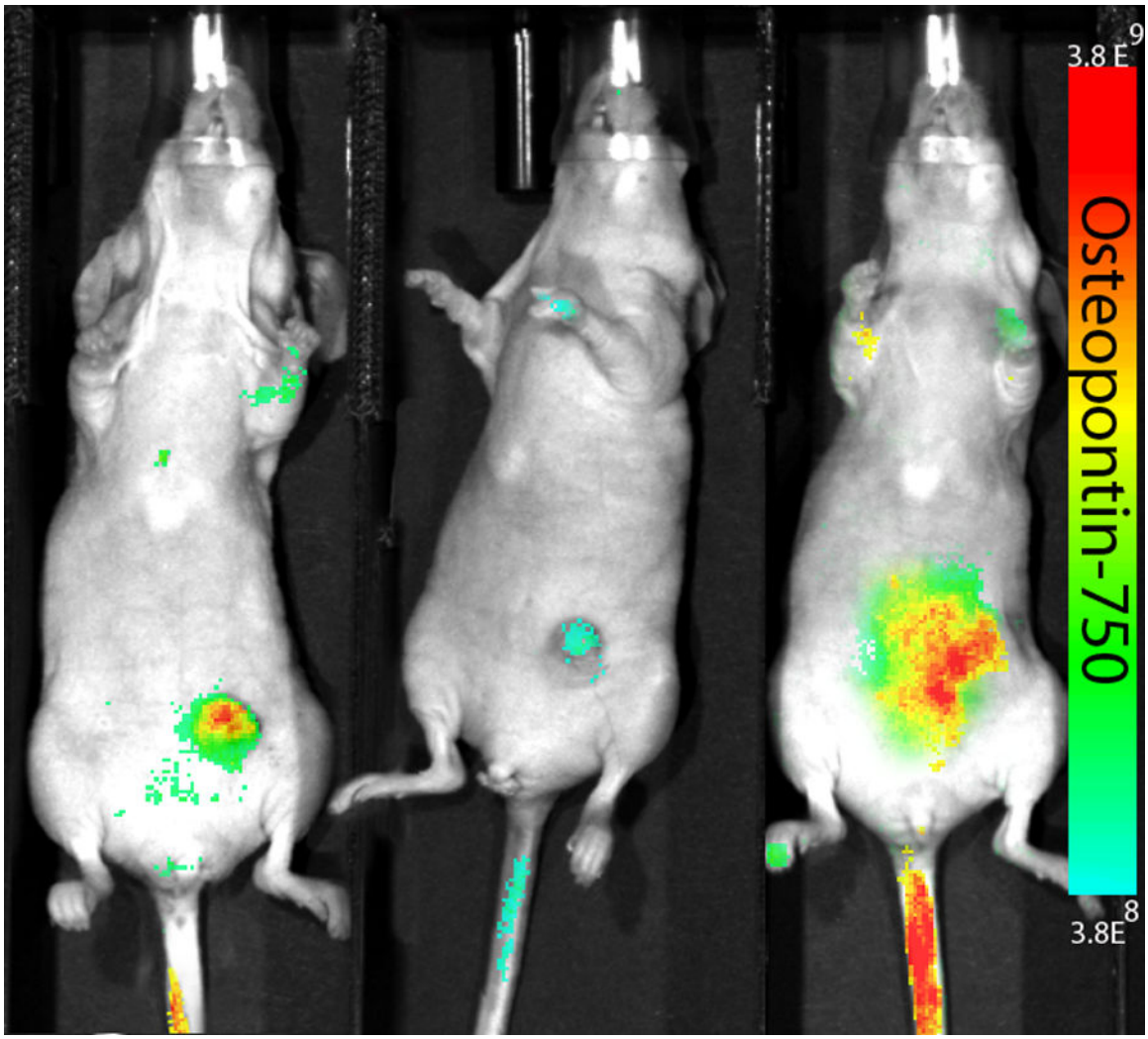

Figure 3.

Near Infrared fluorescent imaging in vivo. MDA-MB-231 cells were orthotopically implanted where tumors grew for 21 days prior to injection of the osteopontin-750 probe. Image shown was acquired at 2 h post osteopontin-750 injection for MSOT and evaluated ex vivo.

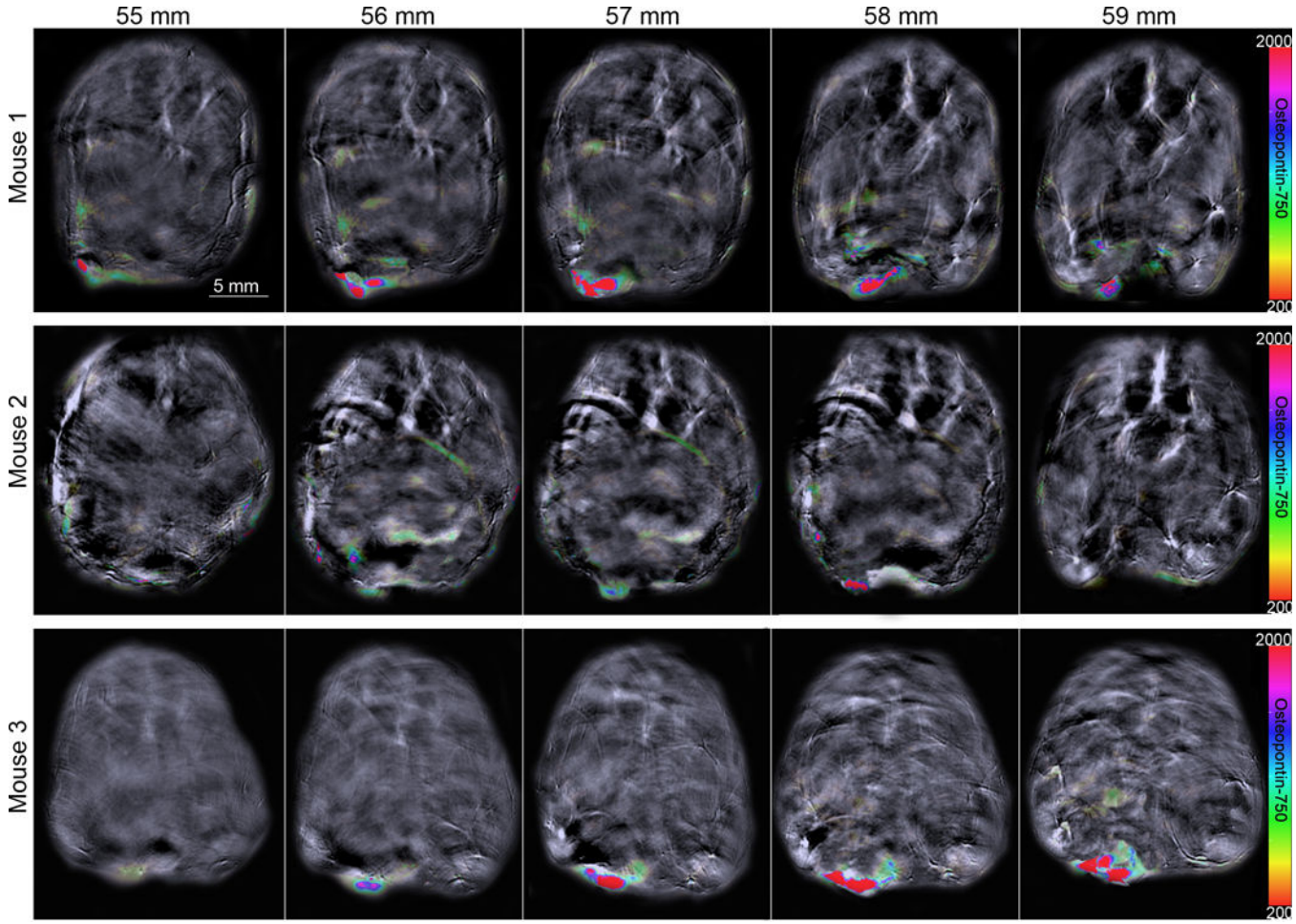

Figure 4.

MSOT in vivo. Accumulation of osteopontin-750 was observed using the rainbow color bar. Background image is shown using 900 nm single wavelength. Images for three mice.

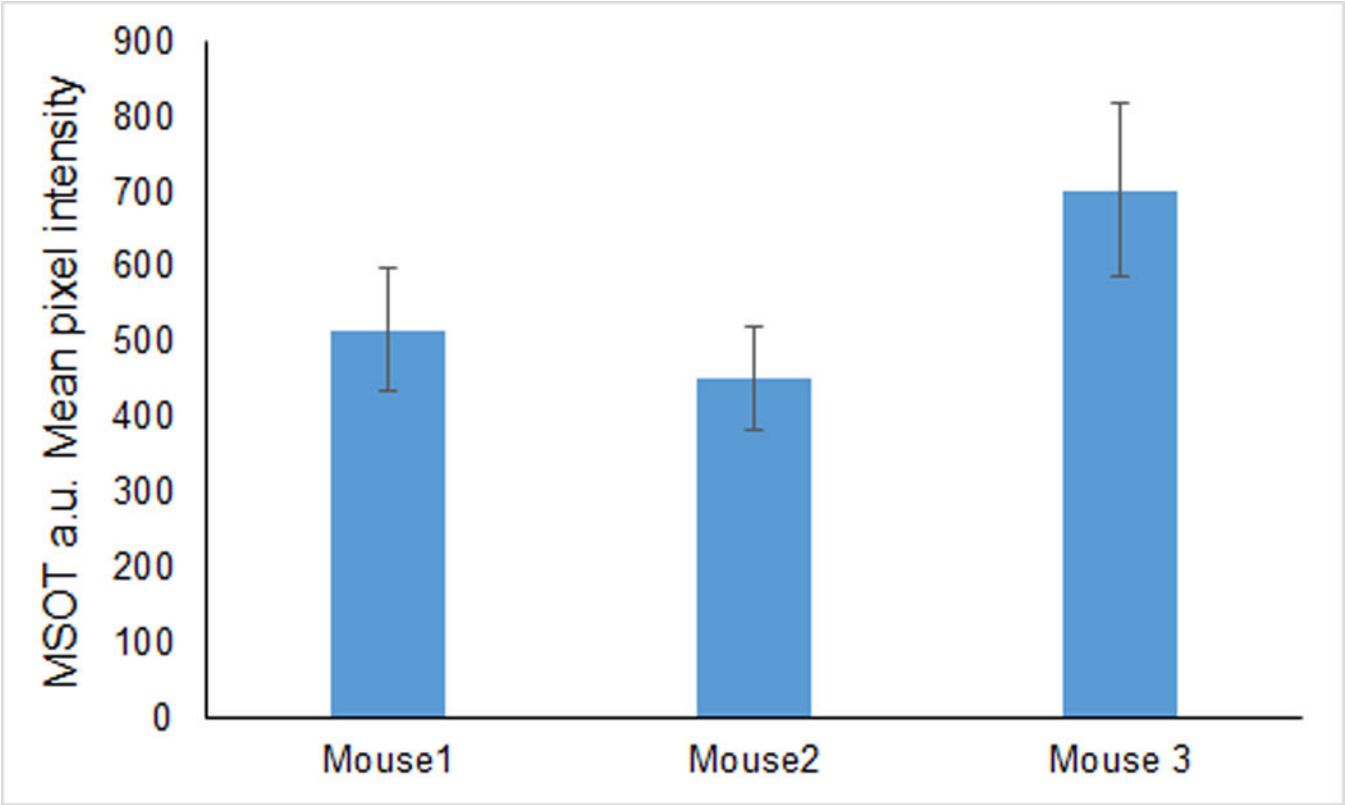

Figure 5.

Group mean osteopontin-750 signal intensity. Mean signal intensity/slice was determined from MSOT images using the ROI method for each of three mice. Data are means ± SD based upon the mean signal intensity for breast tumors among the slices containing tumor.

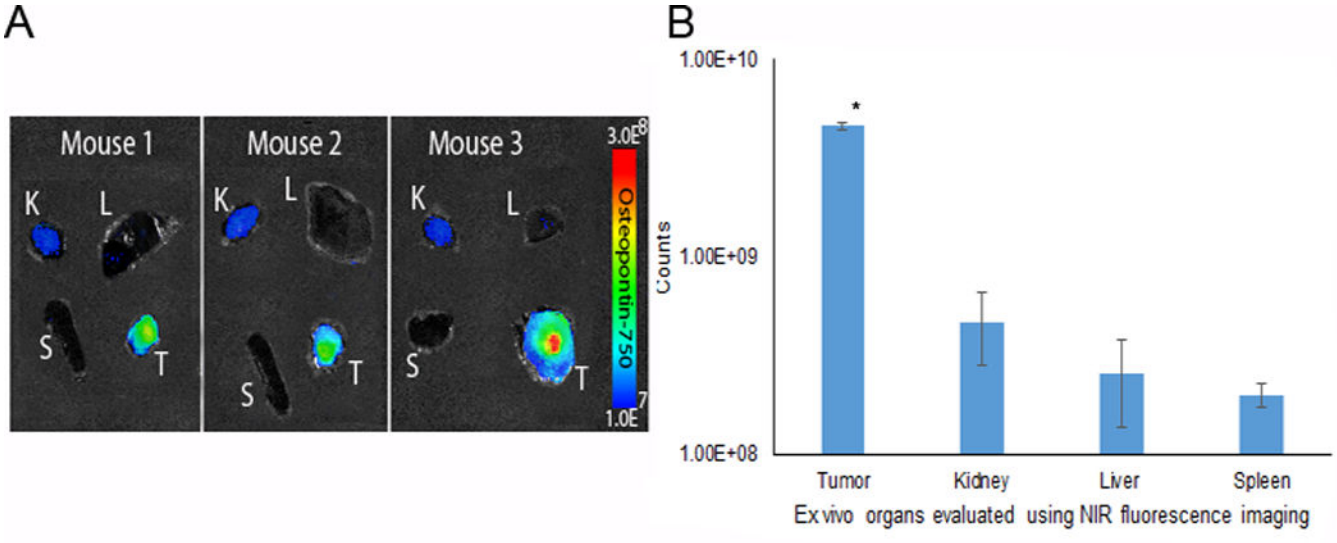

Figure 6.

Secondary confirmation ex vivo using near infrared fluorescent imaging. Imaging demonstrated ex vivo increased probe accumulation within the breast tumor compared to the kidney, liver and spleen at 3 h. A) NIR-fluorescence evaluation of tumor, kidney, liver and spleen using the AMI system indicated that osteopontin-750 accumulated selectively within the breast tumor. B) ROI measurements on organs ex vivo were grouped by organ among three mice. Osteopontin-750 accumulation within the tumor was 4.6×10^9 ($p = 0.0001$) compared to the kidney (4.7×10^8), liver (2.5×10^8) and spleen (2.0×10^8).